Personalized Feature Translation for Expression Recognition: An Efficient Source-Free Domain Adaptation Method

Anonymous authors
Paper under double-blind review

Abstract

Facial expression recognition (FER) models are employed in many video-based affective computing applications, such as human-computer interaction and healthcare monitoring. However, deep FER models often struggle with subtle expressions and high inter-subject variability, limiting their performance in real-world applications. To improve their performance, source-free domain adaptation (SFDA) methods have been proposed to personalize a pretrained source model using only unlabeled target domain data, thereby avoiding data privacy, storage, and transmission constraints. This paper addresses a challenging scenario, where source data is unavailable for adaptation, and only unlabeled target data consisting solely of neutral expressions is available. SFDA methods are not typically designed to adapt using target data from only a single class. Further, using models to generate facial images with non-neutral expressions can be unstable and computationally intensive. In this paper, the Personalized Feature Translation (PFT) method is proposed for SFDA. Unlike current image translation methods for SFDA, our lightweight method operates in the latent space. We first pre-train the translator on the source domain data to transform the subject-specific style features from one source subject into another. Expression information is preserved by optimizing a combination of expression consistency and style-aware objectives. Then, the translator is adapted on neutral target data, without using source data or image synthesis. By translating in the latent space, PFT avoids the complexity and noise of face expression generation, producing discriminative embeddings optimized for classification. Using PFT eliminates the need for image synthesis, reduces computational overhead, and only adapts a lightweight translator, making the method efficient compared to image-based translation. Our extensive experiments[1] on four challenging video FER benchmark datasets, `BioVid`, `StressID`, `BAH`, and `Aff-Wild2`, show that PFT consistently outperforms state-of-the-art SFDA methods, providing a cost-effective approach that is suitable for real-world, privacy-sensitive FER applications.

1 Introduction

FER plays an important role in video-based affective computing, enabling systems to interpret the emotional or health states of humans through non-verbal cues (Calvo & D'Mello, 2010; Ko, 2018). Its applications range from human-computer interaction (Pu & Nie, 2023), to health monitoring (Gaya-Morey et al., 2025), and clinical assessment of pain, depression and stress (Calvo & D'Mello, 2010). Despite recent advances in deep learning (Barros et al., 2019; Sharafi et al., 2022; 2023) and the availability of large annotated datasets for training (Walter et al., 2013; Kollias & Zafeiriou, 2019), deep FER models may perform poorly when deployed on data from new users and operational environments. This is due to the mismatch between distributions of the training (source domain) data and testing (target operational domain) data. Beyond variations in capture conditions, data distributions may differ significantly across subjects. Inter-subject variability (Zeng et al., 2018; Martinez, 2003) can degrade the accuracy and robustness of deep FER models in real-world applications (Li & Deng, 2020a; Zhao et al., 2016).

[1] Our code is included in Appendix and will be made public.

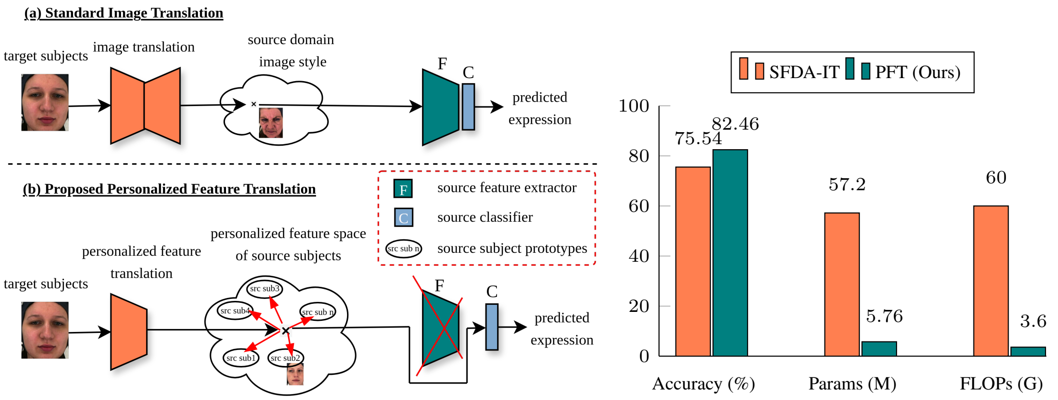
(a) Standard Image Translation
target subjects
image translation
source domain image style
F
C
predicted expression
(b) Proposed Personalized Feature Translation
F source feature extractor
C source classifier
src sub n source subject prototypes
personalized feature translation
personalized feature space of source subjects
target subjects
src sub3
src sub4
src sub n
src sub1
src sub2
F
C
predicted expression
SFDA-IT
PFT (Ours)
100
80
60
40
20
0
75.54
82.46
57.2
5.76
60
3.6
Accuracy (%)
Params (M)
FLOPs (G)

Figure 1: A comparison of standard image translation, SFDA-IT (Hou & Zheng, 2021a), against our proposed personalized feature translation (PFT) for SFDA on `BioVid` data. (a) Image translation methods operate at the pixel level, requiring complex mappings to align target and source styles. (b) Our PFT method translates directly in the feature space using source subject prototypes, allowing for efficient personalization. (*right*) Accuracy, parameter counts, and FLOPs at inference highlight the trade-offs between the two approaches, with models implemented using a `ResNet-18` backbone.

For improved performance, this paper focuses on subject-based adaptation or personalization of deep FER models to video data from target subjects. Various unsupervised domain adaptation (UDA) methods have been proposed to address the distribution shifts by aligning feature distributions (Li & Deng, 2018; Zhu et al., 2016; Chen et al., 2021; Li & Deng, 2020b). However, they typically require access to labeled source data during adaptation, a constraint that is often infeasible in privacy-sensitive application areas like healthcare due to concerns for data privacy, data storage, and computation costs. This has led to the emergence of source-free domain adaptation (SFDA), where adaptation of a pretrained source model is performed using only unlabeled target data (Liang et al., 2020; Tang et al., 2024; Guichemerre et al., 2024). These methods (Fang et al., 2024; Li et al., 2024) can be broadly categorized into (1) model-based approaches, which adapt the model parameters, using target domain statistics or pseudo-labels, and (2) data-based approaches (focus of this paper), which instead operate at the data level by translating target images into the source domain style, enabling inference through the frozen source model without modifying its parameters.

State-of-the-art SFDA methods assume access to data from all target classes, which is not practical in real-world FER applications. Indeed, person-specific data representing non-neutral expressions is typically costly or unavailable. A short neutral control video may, however, be collected for target individuals and used to personalize a model to the variability of an individual's diverse expressions. In practice, collecting and annotating neutral target data for adaptation is generally easier and less subjective than gathering non-neutral emotional data. Recent work has employed GANs to generate expressions based on neutral inputs but relies on image-level disentanglement of identity and expression, which is often unstable and computationally expensive (Sharafi et al., 2025). This limitation reduces the effectiveness of model-based adaptation or fine-tuning strategies, particularly those relying on pseudo-labeling, since labels for neutral data are available during adaptation. However, data-based strategies translate target data into the source domain style. This avoids adapting parameters of the source classifier and enables direct inference with the frozen source model, improving stability, efficiency, and privacy. Following this direction, some SFDA methods (e.g., SFDA-IT) leverage generative models to translate target inputs into source-style images, guided by the source model (Hou & Zheng, 2021a;b). However, these methods are not adapted for subject-specific adaptation of FER models. They consider the source as a single domain and often suppress important subject-specific cues for personalized FER. They also depend on expressive target data, which is rarely available in practice, making generative training infeasible in limited-data settings.

To address the limitations of image translation methods for SFDA, we introduce the Personalized Feature Translation (PFT) method that explicitly models subject-specific variation within the source domain. PFT is a conceptually simple yet effective feature translation method for source-free personalization in FER. The key idea is to pre-train a translator network that maps features from one source subject to another while preserving the underlying expression. This subject-swapping objective encourages the model to capture intra-class, inter-subject variability, learning the structural relationship between expression and identity-specific features within the source domain. During adaptation, only a small subset of the translator's parameters is fine-tuned to translate the style of the target subject, enabling stable and cost-effective personalization. Figure 1 (left) illustrates the difference between image-based and feature-based translation. Image-level methods (Figure 1(a)) generate target images in the source style, relying on complex generative models that introduce instability and high computational overhead. In contrast, Figure 1(b) shows that PFT translates target features directly toward the closest source subject prototypes, preserving expression without pixel-level synthesis. The complexity comparison in Figure 1 (right) shows that PFT achieves higher accuracy while requiring up to 100× fewer parameters and 17× fewer FLOPs than SFDA-IT, highlighting its efficiency and suitability for practical deployment.

Our contributions. **(1)** We propose a personalized feature translation (PFT) method for SFDA in FER using only target images with neutral expressions. Unlike image translation methods that require expressive target data and generative models, our approach translates features across subjects while preserving expression semantics. Adaptation is performed in the feature space with only a small subset of parameters, and a significantly reduction in computational complexity. **(2)** Style-aware and expression consistency losses are proposed to guide the translation process without requiring expressive target data. Our method only requires a few neutral target samples for lightweight adaptation, introduces no additional parameters at inference time, and ensures stable and cost-effective deployment. **(3)** An extensive set of experiments is provided on four video FER benchmarks, `BioVid` (pain estimation), `StressID` (stress recognition), `BAH` (ambivalence-hesitancy recognition), and `Aff-Wild2` (basic expression classification). Results show that our PFT achieves performance that is comparable to or higher than state-of-the-art SFDA (pseudo-labeling and image translation) methods, with lower computational complexity.

2 Related Work

2.1 Facial Expression Recognition

FER aims to identify human emotional states from facial images or video sequences. To enhance generalization, UDA methods (Feng et al., 2023; Cao et al., 2018; Chen et al., 2021; Ji et al., 2019; Li & Deng, 2020b) and multi-source domain adaptation (MSDA) techniques (Zhou et al., 2024) align distributions between source and target domains using unlabeled target data. While effective, these approaches typically require access to source data during adaptation. Personalized FER methods (Yao et al., 2021; Kollias et al., 2020) adapt models to individual users but rely on labeled data per user. More recent subject-aware adaptation frameworks (Zeeshan et al., 2024; 2025) treat each subject as a domain and adapt across users, yet still depend on source data. These constraints motivate the need for SFDA, which enables model personalization without accessing source samples, offering a more practical solution for privacy-sensitive FER applications.

2.2 Source-Free Domain Adaptation and Personalization

SFDA addresses privacy, computational and storage concerns by adapting a pre-trained source model to an unlabeled target domain without access to source data. Common model-based strategies include self-supervised learning (Yang et al., 2021; Litrico et al., 2023), pseudo-labeling (Liang et al., 2020), entropy minimization (Liang et al., 2020), and feature alignment via normalization or auxiliary modules (Li et al., 2016; Liang et al., 2022; Kim et al., 2021b). SHOT (Liang et al., 2020) and DINE (Liang et al., 2022) exemplify efficient adaptation via classifier tuning or BatchNorm statistics. However, these methods often assume confident predictions and smooth domain shifts, which are frequently violated in FER due to high inter-subject variability and subtle expression differences. FER-specific adaptations such as CluP (Conti et al., 2022) and FAL (Zheng et al., 2025) address label noise and pseudo-label instability, yet challenges remain when only neutral target expressions are available. DSFDA (Sharafi et al., 2025) tackles this by disentangling identity and expression using generative models, but its reliance on adversarial training and multi-stage pipelines limits scalability and robustness in practical deployment.

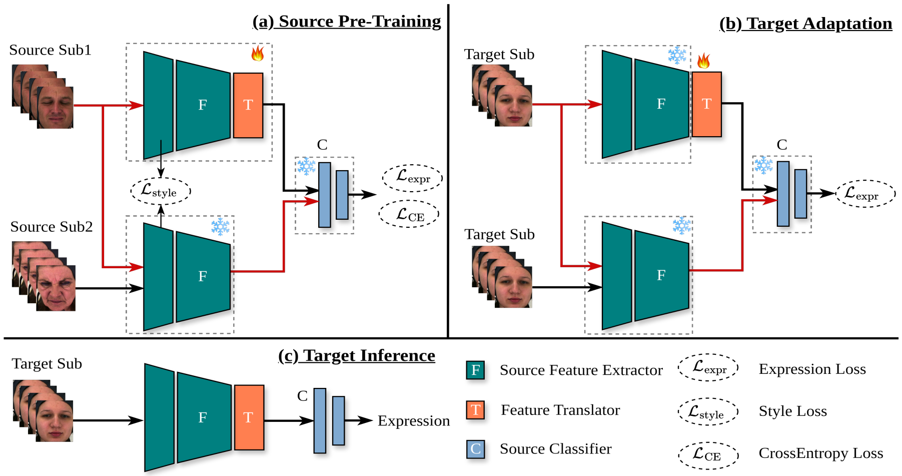
(a) Source Pre-Training
Source Sub1
Source Sub2
F
T
C
$\mathcal{L}_{\text{style}}$
$\mathcal{L}_{\text{expr}}$
$\mathcal{L}_{\text{CE}}$
(b) Target Adaptation
Target Sub
Target Sub
(c) Target Inference
Target Sub
Expression
F Source Feature Extractor
T Feature Translator
C Source Classifier
$\mathcal{L}_{\text{expr}}$ Expression Loss
$\mathcal{L}_{\text{style}}$ Style Loss
$\mathcal{L}_{\text{CE}}$ CrossEntropy Loss

Figure 2: Overview of the proposed PFT method. (a) During pre-training, the translator **T** is trained to map Source Sub1 features into the distribution of Source Sub2, using a combination of style alignment and expression consistency losses. (b) During adaptation, only the feature translator **T** is updated using expression-consistent predictions from two different images (Image1 and Image2) of the same target subject. (c) At inference time, the trained translator **T** and the fixed source classifier **C** are used to predict expression for target-domain inputs.

2.3 Feature Translation for SFDA

Image translation is a common data-based strategy for SFDA that maps target images into the source style using generative models, allowing frozen source models to generalize without access to source data (Hou & Zheng, 2021a;b; Kurmi et al., 2021; Qiu et al., 2021; Tian et al., 2021; Ding et al., 2022). While effective in general tasks, these methods face critical limitations in FER and personalization. FER requires preserving subtle expression cues and identity-specific features, which are often distorted by image synthesis. Moreover, generative models are computationally intensive, prone to instability, and assume access to expressive target samples, an unrealistic assumption in neutral-only personalization settings. To address these challenges, we propose translating features instead of images, using a compact, self-supervised translator that maps target features into the source-aligned space without requiring adversarial training, source data, or expressive target inputs, offering a stable and efficient solution for source-free FER personalization.

3 Proposed Method

Figure 2 illustrates the overall framework of our PFT method. The source model is comprised of a feature extractor backbone and classifier head, both frozen during adaptation. To adapt this model to a new target subject with only a few neutral images extracted from a video, we introduce a translator network, a copy of the source encoder equipped with lightweight adaptation layers after the feature extractor. The translator is pretrained on source data using a subject-swapping objective: translating features between source subjects while maintaining expression labels. This enables the model to capture subject-specific information and preserve expression, facilitating efficient adaptation.

Architecture: Let $\mathcal{D}_S = \{(\mathbf{x}_s, y_s)\}$ be a labeled source dataset, where $\mathbf{x}_s$ is a source subject and $y_s \in \mathcal{Y}$ its corresponding expression label. Let $\mathcal{D}_T = \{\mathbf{x}_t\}$ denote the unlabeled dataset for a target subject. We denote by **F** the source feature extractor and by **C** the classifier head. The translator network is defined as the composition of **F** followed by a set of lightweight, subject-adaptive layers **T**. Thus, the translator $\mathbf{T}_{\text{full}} = \mathbf{T} \circ \mathbf{F}$ takes an image as input and outputs a translated feature representation. The source classifier $(\mathbf{F}, \mathbf{C})$ is trained on $\mathcal{D}_S$ and remains frozen during adaptation. The translator is first pretrained on $\mathcal{D}_S$ to learn identity transformation while preserving expression, and then adapted to each target subject individually using only a few samples.

3.1 Source Pre-Training

The objective of source pre-training is twofold: first, to train a reliable expression classifier on labeled source data, and second, to initialize the translator network so that it can disentangle and recompose identity and expression in the feature space. This initialization is crucial because the translator will later be adapted to new subjects using only a few unlabeled samples.

Formally, the source classifier consists of a feature extractor $\mathbf{F}$ and a classifier head $\mathbf{C}$, which are optimized on the source dataset $\mathcal{D}_S = \{(\mathbf{x}_s, y_s)\}$ by minimizing the standard cross-entropy loss:

$$\mathcal{L}_{\text{CE}}(\mathbf{x}_s, y_s) = -\log \big[\, \mathbf{C}(\mathbf{F}(\mathbf{x}_s)) \,\big]_{y_s}. \tag{1}$$

To pre-train the translator $\mathbf{T}$, we construct pairs of source images $(\mathbf{x}_1, \mathbf{x}_2)$ from distinct subjects. The first image $\mathbf{x}_1$ carries the expression that should be preserved, while the second $\mathbf{x}_2$ provides the target identity to which the representation should adapt. Extracted features are denoted as $\mathbf{f}_1 = \mathbf{F}(\mathbf{x}_1), \mathbf{f}_2 = \mathbf{F}(\mathbf{x}_2), \hat{\mathbf{f}}_1 = \mathbf{T}(\mathbf{f}_1)$. The translated representation $\hat{\mathbf{f}}_1$ is optimized with two complementary criteria. First, expression semantics are preserved by minimizing the divergence between classifier predictions on the original and translated features:

$$\mathcal{L}_{\text{expr}} = D_{\text{KL}}\Big(\mathbf{C}(\mathbf{f}_1) \,\|\, \mathbf{C}(\hat{\mathbf{f}}_1)\Big) \,. \tag{2}$$

Second, the translated feature is explicitly encouraged to adopt the identity statistics of the reference subject $\mathbf{x}_2$. Rather than relying on pixel-level synthesis or adversarial identity matching, we achieve this alignment directly in feature space by matching low-order statistics of early-layer activations. Concretely, for each selected layer $l \in \mathcal{L}$, we compute the per-channel mean $\mu(\cdot)$ and standard deviation $\sigma(\cdot)$ of both the translated representation $\hat{\mathbf{f}}_1^l$ and the reference identity feature $\mathbf{f}_2^l$, and minimize their squared differences. The resulting objective:

$$\mathcal{L}_{\text{style}} = \sum_{l \in \mathcal{L}} \Big(\|\mu(\hat{\mathbf{f}}_1^l) - \mu(\mathbf{f}_2^l)\|_2^2 + \|\sigma(\hat{\mathbf{f}}_1^l) - \sigma(\mathbf{f}_2^l)\|_2^2 \Big), \tag{3}$$

forces the translator to reshape the distribution of $\hat{\mathbf{f}}_1$ so that it reflects the identity-specific style of $\mathbf{x}_2$ while leaving expression semantics intact.

This formulation is inspired by the observation that per-channel statistics encode subject-dependent appearance cues (e.g., facial geometry, texture, or lighting) that are largely orthogonal to expression dynamics. By matching only the first two moments, the translator adapts identity without overfitting to sample-specific details, thus avoiding artifacts that commonly arise in image-level translation. Crucially, this lightweight alignment in feature space is both computationally efficient and robust to noise, making it a key ingredient of our method. The final source pre-training objective combines these components:

$$\mathcal{L}_{\text{source}} = \mathcal{L}_{\text{CE}} + \lambda_{\text{expr}}\, \mathcal{L}_{\text{expr}} + \lambda_{\text{style}}\, \mathcal{L}_{\text{style}}. \tag{4}$$

where λ_{expr} and λ_{style} weight the trade-off between preserving expression semantics and aligning subject identity.

3.2 Target Adaptation and Inference

Given a small set of unlabeled frames from a new target subject, the goal is to personalize the translator $\mathbf{T}_{\text{full}}$ while keeping the source classifier $(\mathbf{F}, \mathbf{C})$ fixed. Adaptation is performed independently for each subject and updates only the lightweight adaptive layers $\mathbf{T}$, ensuring efficiency and avoiding catastrophic interference with previously learned knowledge. Since all target samples originate from the same identity, explicit identity alignment is unnecessary; the adaptation stage thus focuses exclusively on preserving expression semantics. For each target frame $\mathbf{x}_t$, features are first extracted by the frozen source encoder as $\mathbf{f}_t = \mathbf{F}(\mathbf{x}_t)$ and then transformed by the translator as $\hat{\mathbf{f}}_t = \mathbf{T}(\mathbf{f}_t)$.

To maintain expression fidelity, we enforce consistency between classifier predictions before and after translation by minimizing the KL divergence:

$$\mathcal{L}_{\text{expr}} = D_{\text{KL}}\Big(\mathbf{C}(\mathbf{f}_t) \,\|\, \mathbf{C}(\hat{\mathbf{f}}_t)\Big) \,. \tag{5}$$

This self-distillation objective anchors the adapted translator to the original classifier's decision boundary, ensuring that the expression information present in $\mathbf{f}_t$ is preserved after subject-specific transformation. Since labels are not required, even a few neutral frames are sufficient for adaptation. In practice, this enables efficient and data-light personalization that can be performed at test time without revisiting the source dataset.

Inference. After adaptation, the personalized translator $\mathbf{T}_{\text{full}} = \mathbf{T} \circ \mathbf{F}$ is used for recognition. For a new frame $\mathbf{x}_t$ of the same target subject, the translator maps its features into a source-aligned representation while maintaining the subject's expression content. The frozen classifier $\mathbf{C}$ then predicts the expression from the adapted features. This design allows test-time subject personalization without labels, avoids storing or accessing source data during deployment, and eliminates the overhead of pixel-level translation. As a result, the method provides a lightweight yet effective strategy for SFDA in FER, combining the stability of frozen discriminative models with the flexibility of subject-adaptive translation.

4 Results and Discussion

4.1 Experimental Methodology

Datasets: In our experiments, we evaluate on four diverse facial expression datasets: BioVid (Walter et al., 2013), which contains controlled laboratory recordings of pain stimuli; StressID (Chaptoukaev et al., 2023), which captures stress levels based on self-reports; BAH (González-González et al., 2025), a large-scale dataset for recognizing ambivalence and hesitancy expressions in naturalistic recordings; and Aff-Wild2 (Kollias & Zafeiriou, 2019), a widely used in-the-wild benchmark for basic expression recognition. These datasets collectively cover a range of domains, from controlled lab settings to real-world scenarios, and from binary (pain, stress, ambivalence/hesitancy) to multi-class (seven basic emotions) classification tasks. Full dataset descriptions are provided in the Appendix.

Protocol: In experiments, each subject is viewed as an independent target domain. In the BioVid, BAH, Aff-Wild2, and StressID datasets, Following prior works on personalization of FER (Zeeshan et al., 2024; 2025; Sharafi et al., 2025), we evaluate on the standard 10 fixed target subjects used in the literature, which span both genders and cover a range of ages, with each subject contributing hundreds to thousands of frames. This protocol enables fair comparison while ensuring that per-subject metrics are computed over large sample sizes. This subject-specific setup reflects real-world personalization scenarios and enables assessment under inter-subject variability. During adaptation, we assume access only to neutral expression data from the target subjects. No source data are available at this stage, consistent with the SFDA setting. We evaluate performance under the following four settings. **Source-Only.** The model is trained on labeled source-domain data and directly evaluated on target subjects without adaptation. This serves as a lower-bound baseline, highlighting the impact of domain shift. **SFDA (model-based).** The model is adapted using only neutral data from the target domain. We compare our proposed PFT method with recent state-of-the-art SFDA methods, including SHOT (Liang et al., 2020), TPDS (Tang et al., 2024), NRC (Yang et al., 2021), SFIT (Hou & Zheng, 2021b), SFDA-IT (Hou & Zheng, 2021a), and DSFDA (Sharafi et al., 2025). **SFDA (data-based).** This variant incorporates our subject-specific translation module, which aligns target features to the source domain through subject-specific adaptation. **Oracle.** The model is fine-tuned using labeled target-domain data, including neutral and non-neutral expressions.

Implementation Details: Our PFT model was implemented using PyTorch and conducts all experiments on a single NVIDIA A100-SXM4-40GB GPU. The source classifier is built on a ResNet-18 backbone, followed by a classifier trained for binary expression recognition. We select ResNet-18 as the feature extractor due to its widespread adoption in prior FER and domain adaptation works. During target adaptation, only the subject-adaptive layers of the translator are updated; the source backbone and classifier remain fixed. We train the model using the Adam optimizer with a learning rate of 1×10^{-3} and a batch size of 64. We use the learning rate scheduler (ReduceLROnPlateau), which monitors the validation loss and reduces the learning rate by a factor of 0.5 if no improvement is observed for 3 consecutive epochs. We set $\lambda_{\text{expr}} = 1.0$ and $\lambda_{\text{style}} = 0.3$, giving expression preservation higher priority while allowing the style loss to act as a lightweight regularizer for identity alignment.

Table 1: Comparison of the proposed PFT with state-of-the-art SFDA methods on the BioVid dataset (10 target subjects, 77 source subjects). Bold numbers indicate the best F1.

Setting	Methods	Sub-1	Sub-2	Sub-3	Sub-4	Sub-5	Sub-6	Sub-7	Sub-8	Sub-9	Sub-10	Average
Source-only	Source model (no adaptation)	62.78	52.76	82.02	80.83	82.73	56.03	71.85	66.90	50.01	45.79	65.17
SFDA (model-based)	SHOT (Liang et al., 2020)	52.97	45.35	38.98	49.80	51.92	46.43	51.72	46.74	52.10	42.20	47.82
	NRC (Yang et al., 2021)	48.45	32.16	68.60	59.52	65.06	34.85	52.20	44.06	44.82	34.68	48.44
	TPDS (Tang et al., 2024)	62.26	53.16	75.23	64.79	87.06	56.14	58.20	65.84	54.24	45.79	62.27
	DSFDA (Sharafi et al., 2025)	65.72	64.10	77.57	73.12	75.20	57.59	76.15	74.73	59.08	61.54	68.48
SFDA (data-based)	SFIT (Hou & Zheng, 2021b)	76.85	65.33	78.70	80.44	87.01	54.44	57.54	70.81	57.66	**75.92**	70.47
	SFDA-IT (Hou & Zheng, 2021a)	71.54	63.89	84.53	80.30	86.24	59.18	77.66	72.08	54.97	67.01	71.74
	PFT (ours)	**80.65**	**71.75**	**90.26**	**81.54**	**92.68**	**70.06**	**84.26**	**79.29**	**74.53**	58.08	**78.31**
Oracle	Supervised fine-tuning	92.22	86.83	91.89	92.96	91.27	87.65	85.48	90.30	93.28	92.12	90.40

Table 2: Comparison of the proposed PFT with state-of-the-art SFDA methods on the StressID dataset (10 target subjects, 44 source subjects). Bold numbers indicate the best F1.

Setting	Methods	Sub-1	Sub-2	Sub-3	Sub-4	Sub-5	Sub-6	Sub-7	Sub-8	Sub-9	Sub-10	Average
Source-only	Source model (no adaptation)	44.44	43.54	45.34	44.89	45.79	43.99	45.34	44.89	44.44	45.34	44.80
SFDA (model-based)	SHOT (Liang et al., 2020)	42.66	41.79	43.52	43.09	43.95	42.22	43.52	43.09	42.66	43.52	43.00
	NRC (Yang et al., 2021)	40.67	39.85	41.49	41.08	41.90	40.26	41.49	41.08	40.67	41.49	41.00
	TPDS (Tang et al., 2024)	50.10	49.08	51.11	50.60	51.61	49.59	51.11	50.60	50.10	51.11	50.50
	DSFDA (Sharafi et al., 2025)	65.47	64.15	66.79	66.13	67.45	64.81	66.79	66.13	65.47	66.79	66.00
SFDA (data-based)	SFIT (Hou & Zheng, 2021b)	62.00	60.75	63.25	62.63	63.88	61.37	63.25	62.63	62.00	63.25	62.50
	SFDA-IT (Hou & Zheng, 2021a)	63.19	61.91	64.47	63.83	65.10	62.55	64.47	63.83	63.19	64.47	63.70
	PFT (ours)	**69.36**	**67.96**	**70.76**	**70.06**	**71.46**	**68.66**	**70.76**	**70.06**	**69.36**	**70.76**	**69.92**
Oracle	Supervised fine-tuning	96.72	94.76	98.67	97.70	99.65	95.74	98.67	97.70	96.72	98.67	97.50

Table 3: Comparison between the proposed PFT and several state-of-the-art methods on the BAH dataset (10 target subjects, 214 source subjects). Bold numbers indicate the best F1.

Setting	Methods	Sub-1	Sub-2	Sub-3	Sub-4	Sub-5	Sub-6	Sub-7	Sub-8	Sub-9	Sub-10	Average
Source-only	Source model	11.20	17.84	12.60	18.50	14.10	16.92	10.30	13.40	16.00	15.31	14.62
SFDA (model-based)	SHOT (Liang et al., 2020)	40.53	47.91	42.14	46.20	39.81	48.52	41.02	45.70	44.23	45.13	44.10
	NRC (Yang et al., 2021)	48.72	42.30	46.00	44.10	41.81	47.58	43.71	44.65	47.93	44.12	45.00
	TPDS (Tang et al., 2024)	41.22	46.30	44.01	42.54	47.82	40.95	45.53	43.29	47.18	42.23	44.20
	DSFDA (Sharafi et al., 2025)	49.10	44.70	47.51	42.92	50.23	45.30	46.70	47.90	41.82	49.84	46.10
SFDA (data-based)	SFIT (Hou & Zheng, 2021b)	56.83	50.91	54.72	52.10	57.54	49.82	55.91	51.23	58.12	51.40	52.90
	SFDA-IT (Hou & Zheng, 2021a)	48.50	55.71	50.81	53.95	47.21	54.12	49.03	52.64	50.32	**56.00**	51.80
	PFT (Ours)	**61.52**	**55.10**	**60.42**	**53.81**	**59.73**	**56.05**	**61.91**	**54.25**	**62.84**	54.70	**57.40**
Oracle	Supervised fine-tuning	96.20	92.81	95.70	94.25	96.53	93.91	95.14	94.72	92.53	97.01	94.88

4.2 Comparison with State-of-the-Art Methods

For the lab-controlled datasets BioVid and StressID, PFT achieves the highest F1 among all methods (Table 1 and Table 2). On BioVid, which is relatively balanced across classes, PFT obtains an average F1 of 78.31, outperforming DSFDA by almost 10 points. Moreover, to assess robustness across runs, we repeated PFT training on BioVid with three independent seeds and obtained a stable average F1 of 78.43 ± 0.25%, confirming low variance and consistent performance across random initializations. The main failure case is Sub-10, where PFT drops to 58.08. A closer look shows that this subject is from an older age group, where pain-related facial reactions tend to be weaker and more varied. Because of this, the model struggles with recall, even though precision remains high. This indicates that age differences represent a challenge for personalization, consistent with prior FER studies reporting systematically lower recognition accuracy for older adults (Guo et al., 2013; SÖNMEZ, 2019; Kim et al., 2021a), and points to the value of age-aware or group-based adaptation strategies. On StressID, which is strongly imbalanced, PFT reaches 69.92, over 7 points higher than the best competing method, showing that it can handle skewed class distributions while still capturing subject-specific patterns. On the in-the-wild datasets BAH and Aff-Wild2 (Table 3 and Table 4), class imbalance, noisy annotations, and uncontrolled acquisition conditions make F1 a more reliable evaluation metric than accuracy. Here, PFT again delivers the strongest performance, with 57.40 on BAH and 54.46 on Aff-Wild2, outperforming all alternatives. A

Table 4: Comparison between the proposed PFT and several state-of-the-art methods on the Aff-Wild2 dataset (10 target subjects, 282 source subjects). Bold numbers indicate the best F1.

Setting	Methods	Sub-1	Sub-2	Sub-3	Sub-4	Sub-5	Sub-6	Sub-7	Sub-8	Sub-9	Sub-10	Average
Source-only	Source model (no adaptation)	18.70	19.60	20.50	20.00	21.00	20.50	21.40	22.30	20.00	21.00	20.50
SFDA (model-based)	SHOT (Liang et al., 2020)	33.77	34.67	35.57	35.07	36.07	35.57	36.47	37.37	35.07	36.07	35.57
	NRC (Yang et al., 2021)	34.24	35.14	36.04	35.54	36.54	36.04	36.94	37.84	35.54	36.54	36.04
	TPDS (Tang et al., 2024)	36.69	37.59	38.49	37.99	38.99	38.49	39.39	40.29	37.99	38.99	38.49
	DSFDA (Sharafi et al., 2025)	37.26	38.16	39.06	38.56	39.56	39.06	39.96	40.86	38.56	39.56	39.06
SFDA (data-based)	SFIT (Hou & Zheng, 2021b)	48.43	49.33	50.23	49.73	50.73	50.23	51.13	52.03	49.73	50.73	50.23
	SFDA-IT (Hou & Zheng, 2021a)	49.30	50.20	51.10	50.60	51.60	51.10	52.00	52.90	50.60	51.60	51.10
	PFT (ours)	**52.66**	**53.56**	**54.46**	**53.96**	**54.96**	**54.46**	**55.36**	**56.26**	**53.96**	**54.96**	**54.46**
Oracle	Supervised fine-tuning	91.93	92.83	93.73	93.23	94.23	93.73	94.63	95.53	93.23	94.23	93.73

key factor behind this improvement is that PFT operates directly in the feature space, leveraging the robust representations already extracted by the backbone. In contrast, image-translation-based methods attempt to map target samples into a synthetic source domain, often introducing artifacts, blurring, or distortions that suppress subtle but critical expression cues such as micro-expressions or localized muscle activations. These imperfections propagate downstream and degrade classifier performance. By avoiding pixel-level synthesis, PFT preserves discriminative structures in the feature space and provides more stable adaptation under the severe class imbalance and noise characteristic of real-world settings. Full accuracy results are reported in the Appendix, but we emphasize that F1 is a more informative criterion in these imbalanced scenarios.

Table 5: Comparison of SFDA models on BioVid in terms of ACC, number of iterations, and convergence time.

Method	Accuracy (%)	Iters	Time (s)
SFDA-DE (Liang et al., 2020)	62.88	1400	65.5
SHOT (Liang et al., 2020)	50.35	1155	54.0
NRC (Yang et al., 2021)	60.31	705	75.0
PFT (Ours)	**82.46**	**135**	**0.95**

Table 5 compares PFT with representative SFDA methods (SFDA-DE, SHOT, and NRC) in terms of accuracy and adaptation efficiency. All three baselines require substantially more optimization steps and longer convergence times, yet still achieve lower accuracy than PFT. In contrast, our method reaches the highest accuracy with far fewer iterations and under one second of adaptation, highlighting that operating purely in feature space yields a much more efficient and scalable alternative to conventional SFDA optimization.

5 Ablation Studies

Impact of Source Subject Pairing Strategies. To study the effect of source subject pairing during translator pretraining, we evaluate three strategies: random, cosine-based, and landmark-based. Each dataset consists of video recordings, from which we extract individual frames. Faces are detected and center-aligned using 68-point landmarks from Dlib (King, 2009), ensuring spatial consistency across subjects. In the cosine-based strategy, well-classified source samples are paired based on feature similarity in the embedding space, measured via cosine distance. In contrast, the landmark-based strategy leverages facial geometry and pose: facial landmarks are aligned with Procrustes analysis, while head-pose vectors (from OpenFace (Amos et al., 2016)) provide orientation cues. The final similarity score combines landmark and pose differences, with additional constraints on gender and age ($\leq$10 years). As shown in Figure 3, both cosine- and landmark-based pairing outperform random selection, with landmark-based pairing yielding the highest average accuracy across subjects. For the elderly (60+) subject, we also tested an age-aware pairing variant that selects younger expression-matched source references, which improves the F1 score from 58.08% by roughly +7% in our results. Detailed per-subject accuracies are provided the Appendix.

Expression and Identity Specialization in Embeddings. We evaluate the specialization of identity and expression by computing cosine similarities for pairs with (i) the same emotion but different

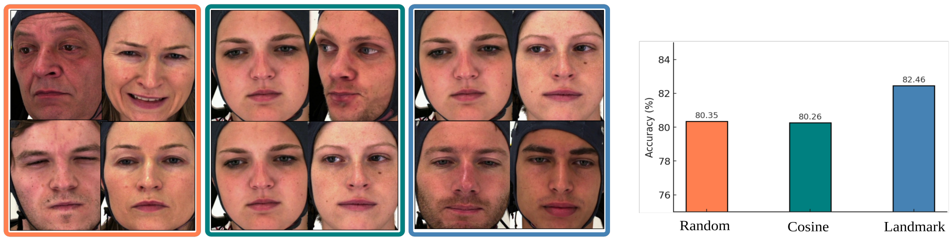

(a) (b)

Figure 3: Source subject pairing on the `BioVid` dataset. (a) Examples of random, cosine-based, and landmark-based pairs. (b) Average `ACC`, with landmark-based pairing performing best.

Table 6: Average target accuracy (%) on `BioVid` using PFT, ablating expression and style losses.

Setting	λ_e	λ_s	**Acc. (%)**
No Losses	✗	✗	68.62
Style Loss	✗	✓	70.10
Expression Loss	✓	✗	71.60
Full Loss	✓	✓	**82.46**

Table 7: Similarity of expression and identity branches on `BioVid`. Fixed expr. means same expression, different subjects, while Fixed subj. means same subject, different expressions.

Branch	Fixed expr.	Fixed subj.
Expression	0.75	0.40
Identity	0.53	0.85

subjects, and (ii) the same subject but different emotions. As shown in Table 7, the expression branch maintains higher similarity for the same emotion (0.75) compared to different emotions (0.40), while the identity branch shows stronger similarity for the same subject (0.85) than for different subjects with the same emotion (0.53). These results show that the expression and identity branches capture primarily emotion and identity features, respectively, with some overlap between them.

Impact of expression and style losses. We analyze the impact of the expression and style losses during source training and their effect on average target classification performance on `BioVid` dataset. As shown in Figure 4, turning off either loss (i.e., setting $\lambda_{\text{expr}}=0$ or $\lambda_{\text{style}}=0$) leads to a substantial drop in accuracy compared to the joint setting, confirming that both components are important for effective translation. The degradation is more pronounced when the style loss is removed, highlighting the dominant role of identity alignment for subject-specific adaptation. At the same time, varying λ_{expr} (with $\lambda_{\text{style}}=0.3$) or λ_{style} (with $\lambda_{\text{expr}}=1.0$) over a broad range yields only modest changes in performance, indicating that PFT is not overly sensitive to moderate perturbations of these hyperparameters around the chosen setting ($\lambda_{\text{expr}}=1.0$, $\lambda_{\text{style}}=0.3$).

Target Sample Distribution Across Source Subjects. To quantify the distribution of target samples and ensure the model doesn't overfit to a single source identity, we use the Nearest Source Prototype Histogram. This visualization shows the cosine similarity between target embeddings and source prototypes, assigning each target sample to the closest source subject. As shown in Figure 5, the histogram reveals a diverse distribution of target samples across multiple source subjects, rather than concentrating on one. This confirms that our model avoids overfitting, promoting better generalization while preserving the variation in identities and expressions across the source domain.

Qualitative Analysis via t-SNE Visualization. In addition, Figure 6 displays t-SNE plots for two complementary views: an *image-based* translation where target samples are first translated in pixel space and then embedded by the frozen backbone, and a *feature-based* translation of PFT that operates directly on latent features. In the image-based plots, translated target clusters remain noticeably shifted away from the source clusters, revealing a larger residual domain gap. By contrast, the PFT plots show target points tightly overlapping the source manifolds, indicating that latent-space translation induces a smaller domain shift while better preserving the underlying expression structure.

Impact of Feature Vector Size on Performance We conducted an ablation study to investigate the impact of feature dimensionality on the performance of feature translation across four FER datasets: `BioVid`, `StressID`, `BAH`, and `Aff-Wild2`. For each dataset, we varied the dimen-

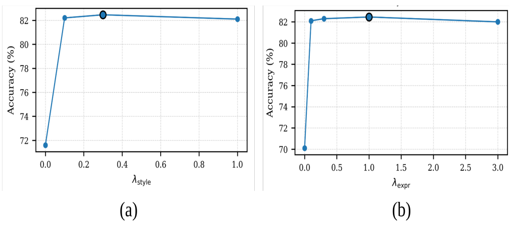

Figure 4: Sensitivity of our PFT method to the expression and style loss weights on BioVid: (a) varying λ_{expr} with λ_{style}=0.3; (b) varying λ_{style} with λ_{expr}=1.0.

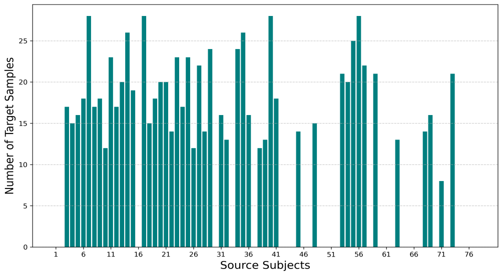

Figure 5: Distribution of target samples for subject 1 in BioVid across source subjects, showing that the translator does not overfit to a single source identity.

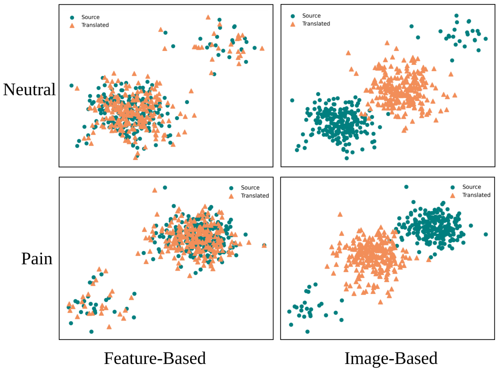

Figure 6: T-SNE of source vs. translated features for Sub-1 in BioVid comparing feature-based (left) and image-based (right) translation.

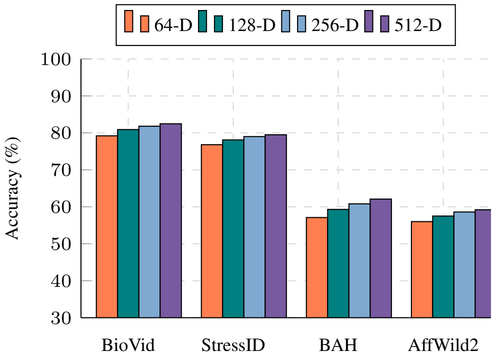

Figure 7: PFT classification ACC across feature dimensions (64–512) on four datasets, showing performance gains with higher dimensions.

sionality of the translated feature vector from 64 to 512 and observed consistent improvements in accuracy with increasing dimensionality. Notably, the performance gains saturated around 256 or 512 dimensions, suggesting that higher-dimensional features provide richer identity and expression information. However, the marginal gains beyond 256 dimensions diminish, indicating a trade-off between representational power and computational efficiency. These trends are illustrated in Figure 7, highlighting the importance of selecting an appropriate feature size for effective and efficient.

6 Conclusion

This paper introduces PFT, an efficient SFDA method tailored for personalization FER using only image data with neutral expressions from target subjects. Unlike traditional image-based approaches that depend on expressive target data and computationally expensive generative models, PFT operates entirely in the feature space. It translates features from one subject to another in the source domain by aligning subject-specific features while preserving the expression of the original subject. This allows the model to maintain the expression of the input while adapting to the source subject, and to provide cost-effective personalization without requiring target expression data. The PFT adaptation process involves adapting only a few layers of the translator module on the target subject's neutral data. PFT is computationally efficient, stable during training, and well-suited for deployment in privacy-sensitive real-world scenarios such as healthcare or mobile applications. Experiments on four video FER datasets shows that PFT can achieve a higher level of performance with lower complexity, generalizing well across both controlled and in-the-wild conditions.

REFERENCES

Brandon Amos, Bartosz Ludwiczuk, and Mahadev Satyanarayanan. Openface: An open source facial behavior analysis toolkit. In *2016 IEEE Winter Conference on Applications of Computer Vision (WACV)*, pp. 1–10. IEEE, 2016.

Pablo Barros, German Parisi, and Stefan Wermter. A personalized affective memory model for improving emotion recognition. In *International Conference on Machine Learning*, pp. 485–494. PMLR, 2019.

Rafael A Calvo and Sidney D'Mello. Affect detection: An interdisciplinary review of models, methods, and their applications. *IEEE Transactions on Affective Computing*, 1(1):18–37, 2010.

Yue Cao, Mingsheng Long, and Jianmin Wang. Unsupervised domain adaptation with distribution matching machines. In *Proceedings of the AAAI conference on artificial intelligence*, volume 32, 2018.

Hava Chaptoukaev, Valeriya Strizhkova, Michele Panariello, Bianca Dalpaos, Aglind Reka, Valeria Manera, Susanne Thümmler, Esma Ismailova, Massimiliano Todisco, Maria A Zuluaga, et al. Stressid: a multimodal dataset for stress identification. *Advances in Neural Information Processing Systems*, 36:29798–29811, 2023.

Tianshui Chen, Tao Pu, Hefeng Wu, Yuan Xie, Lingbo Liu, and Liang Lin. Cross-domain facial expression recognition: A unified evaluation benchmark and adversarial graph learning. *IEEE transactions on pattern analysis and machine intelligence*, 44(12):9887–9903, 2021.

Alessandro Conti, Paolo Rota, Yiming Wang, and Elisa Ricci. Cluster-level pseudo-labelling for source-free cross-domain facial expression recognition. In *Proceedings in the British Machine Vision Conference (BMVC)*, 2022.

Ning Ding, Yixing Xu, Yehui Tang, Chao Xu, Yunhe Wang, and Dacheng Tao. Source-free domain adaptation via distribution estimation. In *Proceedings of the IEEE/CVF conference on computer vision and pattern recognition*, pp. 7212–7222, 2022.

Yuqi Fang, Pew-Thian Yap, Weili Lin, Hongtu Zhu, and Mingxia Liu. Source-free unsupervised domain adaptation: A survey. *Neural Networks*, 174:106230, 2024.

Wei Feng, Lie Ju, Lin Wang, Kaimin Song, Xin Zhao, and Zongyuan Ge. Unsupervised domain adaptation for medical image segmentation by selective entropy constraints and adaptive semantic alignment. In *Proceedings of the AAAI Conference on Artificial Intelligence*, volume 37, pp. 623–631, 2023.

F. Xavier Gaya-Morey, Jose M. Buades-Rubio, Philippe Palanque, Raquel Lacuesta, and Cristina Manresa-Yee. Deep learning-based facial expression recognition for the elderly: A systematic review, 2025. URL `https://arxiv.org/abs/2502.02618`.

Manuela González-González, Soufiane Belharbi, Muhammad Osama Zeeshan, Masoumeh Sharafi, Muhammad Haseeb Aslam, Marco Pedersoli, Alessandro Lameiras Koerich, Simon L Bacon, and Eric Granger. Bah dataset for ambivalence/hesitancy recognition in videos for behavioural change, 2025. URL `https://arxiv.org/abs/2505.19328`.

Alexis Guichemerre, Soufiane Belharbi, Tsiry Mayet, Shakeeb Murtaza, Pourya Shamsolmoali, Luke McCaffrey, and Eric Granger. Source-free domain adaptation of weakly-supervised object localization models for histology. In *Proceedings of the IEEE/CVF Conference on Computer Vision and Pattern Recognition*, pp. 33–43, 2024.

Guodong Guo, Rui Guo, and Xin Li. Facial expression recognition influenced by human aging. *IEEE Transactions on Affective Computing*, 4(3):291–298, 2013.

Yunzhong Hou and Liang Zheng. Source free domain adaptation with image translation, 2021a. URL `https://arxiv.org/abs/2008.07514`.

Yunzhong Hou and Liang Zheng. Visualizing adapted knowledge in domain transfer. In *Proceedings of the IEEE/CVF conference on computer vision and pattern recognition*, pp. 13824–13833, 2021b.

Yanli Ji, Yuhan Hu, Yang Yang, Fumin Shen, and Heng Tao Shen. Cross-domain facial expression recognition via an intra-category common feature and inter-category distinction feature fusion network. *Neurocomputing*, 333:231–239, 2019.

Eugenia Kim, De'Aira Bryant, Deepak Srikanth, and Ayanna Howard. Age bias in emotion detection: An analysis of facial emotion recognition performance on young, middle-aged, and older adults. In *Proceedings of the 2021 AAAI/ACM Conference on AI, Ethics, and Society*, pp. 638–644, 2021a.

Youngeun Kim, Donghyeon Cho, Kyeongtak Han, Priyadarshini Panda, and Sungeun Hong. Domain adaptation without source data. *IEEE Transactions on Artificial Intelligence*, 2(6):508–518, 2021b.

Davis E. King. Dlib-ml: A machine learning toolkit. `http://dlib.net`, 2009. Accessed: 2025-07-31.

Byoung Chul Ko. A brief review of facial emotion recognition based on visual information. *sensors*, 18(2):401, 2018.

Dimitrios Kollias and Stefanos Zafeiriou. Aff-wild2: Extending the aff-wild database for affect recognition, 2019. URL `https://arxiv.org/abs/1811.07770`.

Dimitrios Kollias, Shiyang Cheng, Evangelos Ververas, Irene Kotsia, and Stefanos Zafeiriou. Deep neural network augmentation: Generating faces for affect analysis. *International Journal of Computer Vision*, 128(5):1455–1484, 2020.

Vinod K Kurmi, Venkatesh K Subramanian, and Vinay P Namboodiri. Domain impression: A source data free domain adaptation method. In *Proceedings of the IEEE/CVF winter conference on applications of computer vision*, pp. 615–625, 2021.

Jingjing Li, Zhiqi Yu, Zhekai Du, Lei Zhu, and Heng Tao Shen. A comprehensive survey on source-free domain adaptation. *IEEE Transactions on Pattern Analysis and Machine Intelligence*, 46(8): 5743–5762, 2024.

Shan Li and Weihong Deng. Deep emotion transfer network for cross-database facial expression recognition. In *2018 24th International Conference on Pattern Recognition (ICPR)*, pp. 3092–3099. IEEE, 2018.

Shan Li and Weihong Deng. Deep facial expression recognition: A survey. *IEEE transactions on affective computing*, 13(3):1195–1215, 2020a.

Shan Li and Weihong Deng. A deeper look at facial expression dataset bias. *IEEE Transactions on Affective Computing*, 13(2):881–893, 2020b.

Yanghao Li, Naiyan Wang, Jianping Shi, Jiaying Liu, and Xiaodi Hou. Revisiting batch normalization for practical domain adaptation, 2016. URL `https://arxiv.org/abs/1603.04779`.

Jian Liang, Dapeng Hu, and Jiashi Feng. Do we really need to access the source data? source hypothesis transfer for unsupervised domain adaptation. In *International conference on machine learning*, pp. 6028–6039. PMLR, 2020.

Jian Liang, Dapeng Hu, Jiashi Feng, and Ran He. Dine: Domain adaptation from single and multiple black-box predictors. In *Proceedings of the IEEE/CVF conference on computer vision and pattern recognition*, pp. 8003–8013, 2022.

Mattia Litrico, Alessio Del Bue, and Pietro Morerio. Guiding pseudo-labels with uncertainty estimation for source-free unsupervised domain adaptation. In *Proceedings of the IEEE/CVF Conference on Computer Vision and Pattern Recognition*, pp. 7640–7650, 2023.

Aleix M Martinez. Recognizing expression variant faces from a single sample image per class. In *2003 IEEE Computer Society Conference on Computer Vision and Pattern Recognition, 2003. Proceedings.*, volume 1, pp. I–I. IEEE, 2003.

Jing Pu and Xinxin Nie. Convolutional channel attentional facial expression recognition network and its application in human–computer interaction. *IEEE Access*, 11:129412–129424, 2023.

Zhen Qiu, Yifan Zhang, Hongbin Lin, Shuaicheng Niu, Yanxia Liu, Qing Du, and Mingkui Tan. Source-free domain adaptation via avatar prototype generation and adaptation, 2021. URL `https://arxiv.org/abs/2106.15326`.

Masoumeh Sharafi, Mohammadreza Yazdchi, Reza Rasti, and Fahimeh Nasimi. A novel spatio-temporal convolutional neural framework for multimodal emotion recognition. *Biomedical Signal Processing and Control*, 78:103970, 2022.

Masoumeh Sharafi, Mohammadreza Yazdchi, and Javad Rasti. Audio-visual emotion recognition using k-means clustering and spatio-temporal cnn. In *2023 6th International Conference on Pattern Recognition and Image Analysis (IPRIA)*, pp. 1–6. IEEE, 2023.

Masoumeh Sharafi, Emma Ollivier, Muhammad Osama Zeeshan, Soufiane Belharbi, Marco Pedersoli, Alessandro Lameiras Koerich, Simon Bacon, and Eric Granger. Disentangled source-free personalization for facial expression recognition with neutral target data. In *2025 IEEE 19th International Conference on Automatic Face and Gesture Recognition (FG)*, pp. 1–10, 2025.

ELENA SÖNMEZ. A computational study on aging effect for facial expression recognition. *Turkish Journal of Electrical Engineering and Computer Sciences*, 27(4):2430–2443, 2019.

Song Tang, An Chang, Fabian Zhang, Xiatian Zhu, Mao Ye, and Changshui Zhang. Source-free domain adaptation via target prediction distribution searching. *International journal of computer vision*, 132(3):654–672, 2024.

Jiayi Tian, Jing Zhang, Wen Li, and Dong Xu. Vdm-da: Virtual domain modeling for source data-free domain adaptation. *IEEE Transactions on Circuits and Systems for Video Technology*, 32(6): 3749–3760, 2021.

Steffen Walter, Sascha Gruss, Hagen Ehleiter, Junwen Tan, Harald C Traue, Philipp Werner, Ayoub Al-Hamadi, Stephen Crawcour, Adriano O Andrade, and Gustavo Moreira da Silva. The biovid heat pain database data for the advancement and systematic validation of an automated pain recognition system. In *2013 IEEE international conference on cybernetics (CYBCO)*, pp. 128–131. IEEE, 2013.

Philipp Werner, Ayoub Al-Hamadi, and Steffen Walter. Analysis of facial expressiveness during experimentally induced heat pain. In *2017 Seventh international conference on affective computing and intelligent interaction workshops and demos (ACIIW)*, pp. 176–180. IEEE, 2017.

Shiqi Yang, Joost Van de Weijer, Luis Herranz, Shangling Jui, et al. Exploiting the intrinsic neighborhood structure for source-free domain adaptation. *Advances in neural information processing systems*, 34:29393–29405, 2021.

Anan Yao, Sheng Zhang, and Ruisha Qian. Few-shot learning for personalized facial expression recognition. In *Proceedings of the 29th ACM International Conference on Multimedia*, pp. 2430–2438, 2021.

Muhammad Osama Zeeshan, Muhammad Haseeb Aslam, Soufiane Belharbi, Alessandro Lameiras Koerich, Marco Pedersoli, Simon Bacon, and Eric Granger. Subject-based domain adaptation for facial expression recognition. In *2024 IEEE 18th International Conference on Automatic Face and Gesture Recognition (FG)*, pp. 1–10. IEEE, 2024.

Muhammad Osama Zeeshan, Marco Pedersoli, Alessandro Lameiras Koerich, and Eric Grange. Progressive multi-source domain adaptation for personalized facial expression recognition, 2025. URL `https://arxiv.org/abs/2504.04252`.

Jiabei Zeng, Shiguang Shan, and Xilin Chen. Facial expression recognition with inconsistently annotated datasets. In *Proceedings of the European conference on computer vision (ECCV)*, pp. 222–237, 2018.

Kaili Zhao, Wen-Sheng Chu, and Honggang Zhang. Deep region and multi-label learning for facial action unit detection. In *Proceedings of the IEEE conference on computer vision and pattern recognition*, pp. 3391–3399, 2016.

Ying Zheng, Yiyi Zhang, Yi Wang, and Lap-Pui Chau. Fuzzy-aware loss for source-free domain adaptation in visual emotion recognition. *CoRR*, 2025.

Chaoyang Zhou, Zengmao Wang, Bo Du, and Yong Luo. Cycle self-refinement for multi-source domain adaptation. In *Proceedings of the AAAI Conference on Artificial Intelligence*, volume 38, pp. 17096–17104, 2024.

Ronghang Zhu, Gaoli Sang, and Qijun Zhao. Discriminative feature adaptation for cross-domain facial expression recognition. In *2016 International Conference on Biometrics (ICB)*, pp. 1–7. IEEE, 2016.

Appendix

This supplementary material provides additional insights and evidence supporting the main paper. It includes detailed descriptions of baseline methods, algorithmic procedures, extended experiments on additional datasets, ablation studies analyzing key components, and a summary of hyperparameter configurations used in our evaluations.

A Algorithm Details

This section outlines the core procedures of our proposed Personalized Feature Translation (PFT) framework for SFDA. The method comprises two stages: (1) source pre-training, and (2) target-domain. The full pseudocode is provided in Algorithms 1 and 2, and we define the main notations below.

Architecture: Let $\mathcal{D}_S = \{(\mathbf{x}_s, y_s)\}$ be a labeled source dataset, where $\mathbf{x}_s$ is a source subject and $y_s \in \mathcal{Y}$ its corresponding expression label. Let $\mathcal{D}_T = \{\mathbf{x}_t\}$ denote the unlabeled dataset for a target subject. We denote by $\mathbf{F}$ the source feature extractor and by $\mathbf{C}$ the classifier head. The translator network is defined as the composition of $\mathbf{F}$ followed by a set of lightweight, subject-adaptive layers $\mathbf{T}$. Thus, the translator $\mathbf{T}_{\text{full}} = \mathbf{T} \circ \mathbf{F}$ takes an image as input and outputs a translated feature representation. The source classifier $(\mathbf{F}, \mathbf{C})$ is trained on $\mathcal{D}_S$ and remains frozen during adaptation. The translator is first pretrained on $\mathcal{D}_S$ to learn identity transformation while preserving expression, and then adapted to each target subject individually using only a few samples.

Algorithm 1 Source Pre-training

```
procedure PretrainSource($\mathcal{D}_S, \mathbf{F}, \mathbf{C}, \mathbf{T}$)
    Initialize $\mathbf{F}, \mathbf{C}, \mathbf{T}$
    for each epoch do
        for all $(\mathbf{x}_s, y_s) \in \mathcal{D}_S$ do
            $\mathbf{f}_s \leftarrow \mathbf{F}(\mathbf{x}_s)$
            $y_{\text{pred}} \leftarrow \mathbf{C}(\mathbf{f}_s)$
            $\mathcal{L}_{\text{CE}} \leftarrow \text{CrossEntropy}(y_{\text{pred}}, y_s)$
            Update $\mathbf{F}, \mathbf{C}$ using $\mathcal{L}_{\text{CE}}$
        end for
    end for
    Freeze $\mathbf{F}$
    for each epoch do
        for all paired $(\mathbf{x}_1, y_1), (\mathbf{x}_2, \cdot) \in \mathcal{D}_S$ do
            $\mathbf{f}_1 \leftarrow \mathbf{F}(\mathbf{x}_1)$
            $\mathbf{f}_2 \leftarrow \mathbf{F}(\mathbf{x}_2)$
            $\hat{\mathbf{f}}_1 \leftarrow \mathbf{T}(\mathbf{f}_1)$
            $\mathcal{L}_{\text{expr}} \leftarrow D_{\text{KL}}(\mathbf{C}(\mathbf{f}_1) \parallel \mathbf{C}(\hat{\mathbf{f}}_1))$
            $\mathcal{L}_{\text{style}} \leftarrow 0$
            for all $l \in \mathcal{L}$ do
                $\mu_1, \sigma_1 \leftarrow \text{MeanStd}(\hat{\mathbf{f}}_1^l)$
                $\mu_2, \sigma_2 \leftarrow \text{MeanStd}(\mathbf{f}_2^l)$
                $\mathcal{L}_{\text{style}} \leftarrow \mathcal{L}_{\text{style}} + \|\mu_1 - \mu_2\|^2 + \|\sigma_1 - \sigma_2\|^2$
            end for
            $\mathcal{L}_{\text{CE}} \leftarrow \text{CrossEntropy}(\mathbf{C}(\hat{\mathbf{f}}_1), y_1)$
            $\mathcal{L}_{\text{total}} \leftarrow \mathcal{L}_{\text{CE}} + \lambda_{\text{expr}} \cdot \mathcal{L}_{\text{expr}} + \lambda_{\text{style}} \cdot \mathcal{L}_{\text{style}}$
            Update $\mathbf{T}$ using $\mathcal{L}_{\text{total}}$
        end for
    end for
end procedure
```

Algorithm 2 Target Adaptation

```
procedure AdaptToTarget($\mathcal{D}_T, \mathbf{F}, \mathbf{C}, \mathbf{T}$)
    Freeze $\mathbf{F}, \mathbf{C}$
    for each epoch do
        for all $\mathbf{x}_t \in \mathcal{D}_T$ do
            $\mathbf{f}_t \leftarrow \mathbf{F}(\mathbf{x}_t)$
            $\hat{\mathbf{f}}_t \leftarrow \mathbf{T}(\mathbf{f}_t)$
            $\mathcal{L}_{\text{expr}} \leftarrow D_{\text{KL}}(\mathbf{C}(\mathbf{f}_t) \parallel \mathbf{C}(\hat{\mathbf{f}}_t))$
            Update $\mathbf{T}$ using $\mathcal{L}_{\text{expr}}$
        end for
    end for
end procedure
```

B Baseline Method Descriptions

We compare our proposed method against seven representative SFDA baselines. These methods span both feature-space and image-space adaptation strategies, enabling a comprehensive evaluation of our approach. For fairness, all baselines are implemented using a fixed `ResNet-18` backbone and evaluated under a consistent experimental protocol.

- **SHOT** (Liang et al., 2020) freezes the source feature extractor and adapts only the classifier using pseudo-labeling and information maximization, encouraging discriminative clustering in the target domain without accessing source data.

- **TPDS** (Tang et al., 2024) introduces a progressive adaptation framework that bridges source and target domains via a series of proxy distributions, aligning predictions using category consistency and mutual information objectives.
- **NRC** (Yang et al., 2021) exploits the intrinsic neighborhood structure of the target data by enforcing label consistency among reciprocal neighbors, using a memory bank for efficient retrieval.
- **DSFDA** (Sharafi et al., 2025) adapts FER models using only neutral target videos by disentangling identity and expression features, generating synthetic expressive data, and jointly training in a one-stage framework.
- **SFIT** (Hou & Zheng, 2021b) visualizes the knowledge gap between source and target models by translating target images into source-style images using only the two model checkpoints. It employs a generator guided by knowledge distillation and a relationship-preserving loss, enabling adaptation and fine-tuning without source data.
- **SFDA-IT** (Hou & Zheng, 2021a) formulates domain adaptation as an image translation problem where a generator maps target images into source-style images without paired supervision. The translated images are then classified by the fixed source model, improving performance through batch-wise style alignment and entropy regularization.

C Extended Experimental Results

C.1 Datasets

- `BioVid`: Heat and Pain (Part A): This dataset (Walter et al., 2013) consists of video recordings of 87 subjects experiencing thermal pain stimuli in a controlled laboratory setting. Each subject is assigned to one of five pain categories: “no pain” and four increasing pain levels (PA1–PA4), with PA4 representing the highest intensity. Consistent with prior work, which reports minimal facial activity at lower intensities, we focus on a binary classification between “no pain” and PA4. For each subject, 20 videos per class are used, each lasting 5.5 seconds. Following recommendations in (Werner et al., 2017), the first 2 seconds of each PA4 video are discarded to eliminate frames where facial expressions are typically absent, retaining only the segments that capture stronger pain-related facial activity.

- `StressID`: This dataset (Chaptoukaev et al., 2023) focuses on assessing stress through facial expressions. It comprises facial video recordings from 54 individuals, totaling around 918 minutes of annotated visual content. In our work, we use only the visual modality. Each frame is labeled as either “neutral” or “stressed,” based on participants’ self-reported stress scores. Specifically, frames corresponding to scores below 5 are labeled as neutral (label 0), while those with scores of 5 or higher are considered stressed (label 1).

- `BAH`: The `BAH` dataset (González-González et al., 2025), which is designed for recognizing ambivalence and hesitancy (A/H) expressions in real-world video recordings.comprises facial recordings from 224 participants across Canada, designed to reflect a diverse demographic distribution in terms of sex, ethnicity, and province. Each participant contributes up to seven videos, with a total of 1,118 videos (86.2 hours). Among these, 638 videos contain at least one A/H segment, resulting in a total of 1,274 annotated A/H segments. The dataset includes 143,103 frames labeled with A/H, out of 714,005 total frames. In our setup, frames with A/H annotations are assigned a label of 1 (indicating the presence of A or H), while all other frames are considered neutral and assigned a label of 0.

- `Aff-Wild2`: The `Aff-Wild2` dataset (Kollias & Zafeiriou, 2019) is a large-scale in-the-wild dataset for affect recognition, consisting of 318 videos with available annotations. In our study, we use a subset of 292 videos that each represent a single subject, which is essential for our subject-based setting, where each individual is treated as a separate domain. We focus exclusively on basic expression categories for discrete expression classification. Specifically, we use the following seven classes: neutral (0), anger (1), disgust (2), fear (3), happiness (4), sadness (5), and surprise (6). We consider only the visual modality in our experiments.

Table 8: Comparison of the proposed PFT with state-of-the-art SFDA methods on the `BioVid` dataset (10 target subjects, 77 source subjects). All models use `ResNet-18`. Bold numbers indicate the best `ACC`.

Setting	**Methods**	**Sub-1**	**Sub-2**	**Sub-3**	**Sub-4**	**Sub-5**	**Sub-6**	**Sub-7**	**Sub-8**	**Sub-9**	**Sub-10**	**Average**
Source-only	Source model (no adaptation)	66.11	55.55	86.36	85.11	87.11	59.00	75.66	70.44	52.66	48.22	68.62
SFDA (model-based)	SHOT (Liang et al., 2020)	55.78	47.76	41.05	52.44	54.67	48.89	54.46	49.22	54.86	44.44	50.35
	NRC (Yang et al., 2021)	59.33	39.38	84.00	72.89	79.67	42.67	63.92	53.95	54.89	42.47	60.31
	TPDS (Tang et al., 2024)	65.56	55.98	79.22	68.22	91.67	59.11	61.28	69.33	57.11	48.22	65.57
	DSFDA (Sharafi et al., 2025)	77.00	75.11	90.89	85.67	88.11	67.48	89.22	**87.56**	69.22	72.11	80.24
SFDA (data-based)	SFIT (Hou & Zheng, 2021b)	80.92	68.79	82.87	84.70	91.62	57.32	60.59	74.56	60.71	**79.94**	74.20
	SFDA-IT (Hou & Zheng, 2021a)	75.33	67.27	89.00	84.55	90.80	62.31	81.77	75.89	57.88	70.56	75.54
	PFT (ours)	**84.93**	**75.56**	**95.05**	**85.86**	**97.59**	**73.78**	**88.73**	83.49	**78.48**	61.16	**82.46**
Oracle	Fine-Tuning	97.11	91.43	96.76	97.89	96.11	92.30	90.01	95.09	98.22	97.00	95.19

Table 9: Comparison of the proposed PFT with state-of-the-art SFDA methods on the `StressID` dataset (10 target subjects, 44 source subjects). All models use `ResNet-18`. Bold numbers indicate the best `ACC`.

Setting	**Methods**	**Sub-1**	**Sub-2**	**Sub-3**	**Sub-4**	**Sub-5**	**Sub-6**	**Sub-7**	**Sub-8**	**Sub-9**	**Sub-10**	**Average**
Source-only	Source model (no adaptation)	38.96	41.21	65.53	42.04	55.16	65.51	69.43	60.78	53.62	55.63	54.79
SFDA (model-based)	SHOT (Liang et al., 2020)	68.33	51.95	45.83	39.26	53.67	61.38	59.76	45.25	51.42	52.05	52.88
	NRC (Yang et al., 2021)	69.03	52.25	31.83	35.29	59.67	42.50	59.28	41.25	65.42	54.20	51.07
	TPDS (Tang et al., 2024)	65.56	54.98	64.22	58.22	54.67	63.11	69.28	59.33	50.11	51.98	59.17
	DSFDA Sharafi et al. (2025)	73.47	69.39	**87.12**	69.74	79.87	87.39	82.80	83.89	**75.03**	77.39	78.61
SFDA (data-based)	SFIT (Hou & Zheng, 2021b)	70.41	68.85	69.67	71.92	67.48	77.43	70.76	75.21	65.98	61.19	69.89
	SFDA-IT (Hou & Zheng, 2021a)	73.47	69.50	69.90	73.02	66.54	78.62	71.30	76.67	65.42	67.32	71.18
	PFT (ours)	**78.33**	**74.87**	78.17	**73.32**	**79.96**	**89.00**	**84.76**	**84.14**	74.42	**77.95**	**79.49**
Oracle	Fine-Tuning	98.89	100	99.53	98.15	99.22	97.57	96.02	99.38	99.56	100	98.83

C.2 Quantitative Comparison with SFDA Baselines

Across the lab-controlled datasets `BioVid` and `StressID`, our proposed PFT achieves the best performance compared to all baselines (Table 8 and Table 9). On `BioVid`, PFT improves the average accuracy to 82.46%, surpassing the best baseline (SFDA-TT) by more than 2 percentage points. Similarly, on `StressID`, PFT reaches 71.49%, again outperforming all competing methods. These gains highlight the advantage of PFT in settings where acquisition conditions are stable, allowing feature-level adaptation to capture subtle subject-specific differences with reduced variance across individuals. While overall performance is strong, two notable failure cases appear on `BioVid` for Sub-8 and Sub-10, where PFT achieves only 83.49% and 61.16%, respectively. Both subjects belong to the older age group, where pain-related facial responses are less pronounced and more variable, reducing the discriminability of features. This suggests that subject age can act as a confounding factor in personalized adaptation and points to the potential benefit of future age-aware or stratified domain adaptation strategies.

On the more in-the-wild datasets `BAH` and `Aff-Wild2`, PFT remains highly competitive (Table 10 and Table 11). On `BAH`, PFT clearly outperforms all alternatives, achieving 62.09% average accuracy, over 4 points higher than the best image-translation baseline. On `Aff-Wild2`, which involves 7 classes and severe real-world noise, PFT performs on par with the strongest baseline, trailing by less than 1 percentage point. The remaining gap arises from multi-class confusion and extreme conditions such as pose variation, motion blur, and class imbalance. Notably, PFT surpasses image-translation-based methods because it adapts directly in the feature space rather than the image space: image translation often introduces artifacts or loses discriminative details (e.g., subtle muscle activations or micro-expressions), which weakens downstream classification. By preserving the discriminative structure already extracted by the backbone, PFT avoids error accumulation from imperfect translations and provides more stable, reliable adaptation across subjects.

C.3 Qualitative Examples of SFDA-IT Translations

In addition to quantitative results, we also provide qualitative examples of translated images generated by SFDA-IT (Hou & Zheng, 2021a). As an image-based adaptation method, SFDA-IT (Hou

Table 10: Comparison between the proposed PFT and several state-of-the-art methods on the `BAH` dataset (10 target subjects, 214 source subjects). All models use `ResNet-18`. Bold numbers indicate the best `ACC`.

Setting	Methods	Sub-1	Sub-2	Sub-3	Sub-4	Sub-5	Sub-6	Sub-7	Sub-8	Sub-9	Sub-10	Average
Source-only	Source model	49.71	50.00	54.67	47.71	48.43	51.51	48.83	50.30	50.45	48.65	50.03
SFDA (model-based)	SHOT (Liang et al., 2020)	49.73	54.17	**60.49**	49.55	45.83	51.22	46.62	52.76	49.09	47.92	50.74
	NRC (Yang et al., 2021)	49.46	54.05	55.02	49.11	46.52	49.91	44.83	52.26	48.63	47.24	49.70
	TPDS (Tang et al., 2024)	50.42	52.38	55.91	48.75	47.67	51.66	44.83	53.20	51.75	55.13	51.17
	DSFDA (Sharafi et al., 2025)	61.24	56.02	60.31	58.77	54.19	59.88	**57.40**	53.16	62.15	60.49	58.36
SFDA (data-based)	SFIT (Hou & Zheng, 2021b)	60.15	56.84	60.04	54.91	56.15	55.73	56.02	56.49	56.22	58.39	57.09
	SFDA-IT (Hou & Zheng, 2021a)	60.00	60.12	56.48	55.73	56.15	57.42	56.80	55.96	56.89	57.05	57.26
	PFT (Ours)	**69.46**	**64.17**	**60.49**	**62.11**	**59.83**	**61.91**	54.62	**57.76**	**62.63**	**67.92**	**62.09**
Oracle	Fine-tune	93.35	96.61	99.22	95.58	99.17	97.89	92.48	96.14	93.07	93.38	95.69

Table 11: Comparison between the proposed PFT and several state-of-the-art methods on the `Aff-Wild2` dataset (10 target subjects, 282 source subjects). All models use `ResNet-18`. Bold numbers indicate the best `ACC`.

Setting	Methods	Sub-1	Sub-2	Sub-3	Sub-4	Sub-5	Sub-6	Sub-7	Sub-8	Sub-9	Sub-10	Average
Source-only	Source model	24.50	23.97	21.94	30.17	32.41	40.63	16.92	37.67	18.77	19.98	26.70
SFDA (model-based)	SHOT (Liang et al., 2020)	45.00	41.67	40.42	43.91	39.88	41.34	42.18	39.00	49.16	50.84	42.34
	NRC (Yang et al., 2021)	43.77	42.31	40.98	44.26	41.83	40.61	42.12	43.29	49.12	50.71	42.90
	TPDS (Tang et al., 2024)	47.62	44.18	43.75	46.03	42.87	41.59	44.22	41.07	49.08	50.49	45.09
	DSFDA (Sharafi et al., 2025)	58.31	56.78	57.96	59.24	55.63	58.09	56.41	57.18	57.82	56.18	57.42
SFDA (data-based)	SFIT (Hou & Zheng, 2021b)	58.42	56.37	54.79	57.61	55.03	52.98	56.85	57.12	49.56	50.57	55.93
	SFDA-IT (Hou & Zheng, 2021a)	59.63	57.88	54.42	58.07	53.61	55.94	50.83	55.76	58.23	**56.83**	56.12
	PFT (Ours)	**60.83**	**59.47**	**58.26**	**61.72**	**57.39**	**60.91**	**56.18**	**59.64**	**61.05**	56.75	**59.20**
Oracle	Fine-tune	98.90	98.71	98.03	98.37	94.66	83.33	99.87	81.48	94.54	97.88	94.58

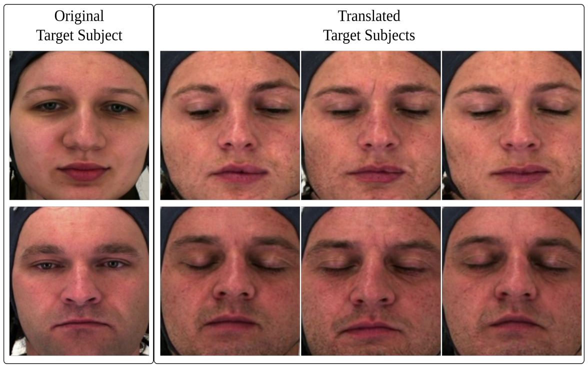

Figure 8: Translated images of two target subjects from the `BioVid` dataset using landmark pairs at test time with the SFDA-IT (Hou & Zheng, 2021a) method. *Left* column shows the original target image. *Right* columns display the corresponding translated images used for classification.

& Zheng, 2021a) maps target-domain samples into a source-style visual space before classification. Figure 8 illustrates representative examples from `BioVid`, showing target input frames and their translated counterparts. While SFDA-IT (Hou & Zheng, 2021a) effectively alters low-level style features, it may fail to preserve fine-grained facial expressions essential for accurate classification, particularly in subtle affective states.

D Additional Ablation Studies

D.1 Distribution of Distances to Closest Sources After Translation

To assess the effectiveness of our subject-aware translation module, we plot the L2 distances between translated target samples and the closest source subject prototype in the feature space. As

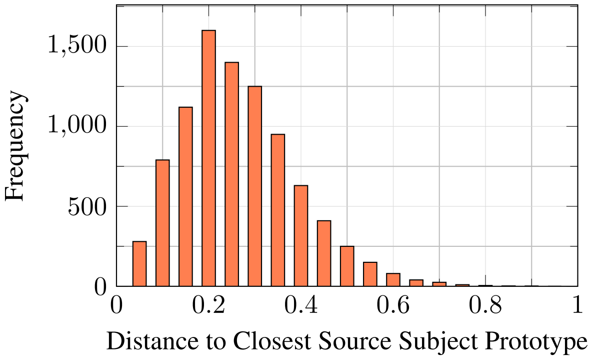

Figure 9: Histogram of distances between translated target frames and their closest source prototype.

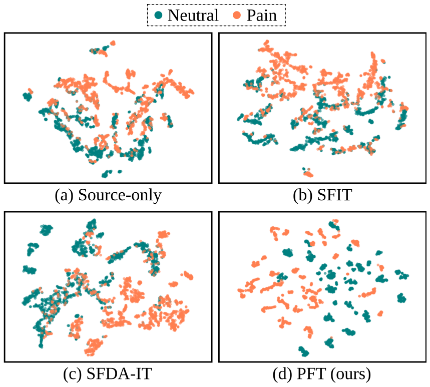

(a) Source-only (b) SFIT (c) SFDA-IT (d) PFT (ours)

Figure 10: t-SNE visualizations before and after PFT adaptation for Sub-1 in `BioVid` dataset.

shown in Figure 9, the distribution is asymmetric, with a strong concentration of distances around 0.2 and a long tail toward higher values. This indicates that most translated target features are successfully aligned close to their corresponding source subject representations, validating the role of the translation mechanism in enhancing subject-level alignment. The sharp peak and reduced spread reflect improved intra-class compactness and inter-domain consistency, which are critical for minimizing domain shift in source-free adaptation settings.

D.2 Qualitative Analysis via t-SNE visualization.

Target embeddings are visualized using t-SNE for a representative subject (Sub-1) across four models, source-only, SFIT (Hou & Zheng, 2021b)(b), SFDA-IT (Hou & Zheng, 2021a), and our PFT (Figure. 10). Initially, the source-only model (a) yields overlapping neutral/pain clusters. After adaptation, SFIT (b) adds mild structure but remains mixed; SFDA-IT (c) shows clearer yet diffuse boundaries; PFT (d) forms compact, well-separated clusters, indicating better expression preservation and domain alignment.

D.3 Impact of Feature Vector Size on Performance

We conducted an ablation study to investigate the impact of feature dimensionality on the performance of feature translation across four FER datasets: `BioVid`, `StressID`, `BAH`, and `Aff-Wild2`. For each dataset, we varied the dimensionality of the translated feature vector from 64 to 512 and observed consistent improvements in accuracy with increasing dimensionality. Notably, the performance gains saturated around 256 or 512 dimensions, suggesting that higher-dimensional features provide richer identity and expression information. However, the marginal gains beyond 256 dimensions diminish, indicating a trade-off between representational power and computational efficiency. These trends are illustrated in Figure 7, highlighting the importance of selecting an appropriate feature size for effective and efficient.

D.4 Effect of Backbone Architecture

To assess whether the gains of PFT depend on a particular backbone, we repeat all experiments with both a transformer encoder (`ViT-B/32`) and a convolutional encoder (`ResNet-50`) across `BioVid`, `StressID`, and `BAH`. In all settings, PFT achieves the best average `F1` and yields the highest or near-highest subject-wise performance (Tables 12–17), outperforming SHOT, DSFDA, SFIT, and SFDA-IT. These results indicate that the proposed feature-space translation is robust to the choice of backbone and can be used as a plug-and-play SFDA module for both CNN- and ViT-based FER models.

Table 12: Comparison of the proposed PFT with state-of-the-art SFDA methods on the BioVid dataset (10 target subjects, 77 source subjects) with ViT-B/32 . Bold numbers indicate the best F1.

Methods	**Sub-1**	**Sub-2**	**Sub-3**	**Sub-4**	**Sub-5**	**Sub-6**	**Sub-7**	**Sub-8**	**Sub-9**	**Sub-10**	**Average**
Src_only	68.89	52.00	85.00	74.56	75.00	56.69	65.89	56.00	64.55	59.55	65.81
SHOT	69.99	66.00	82.14	75.69	79.69	57.00	69.00	74.69	69.00	61.60	70.48
DSFDA	70.16	66.52	85.99	81.11	85.66	64.36	78.22	75.00	67.23	63.00	73.72
SFIT	70.16	69.00	86.55	80.69	81.45	63.60	80.00	74.66	65.36	61.00	73.24
SFDA-IT	69.99	71.00	88.00	80.90	86.97	66.00	79.65	64.56	66.47	60.98	73.45
PFT (Ours)	**77.00**	**71.00**	**90.20**	**81.50**	**88.10**	**67.50**	**84.60**	**75.20**	**68.00**	**63.40**	**76.65**

Table 13: Comparison of the proposed PFT with state-of-the-art SFDA methods on the StressID dataset (10 target subjects, 44 source subjects) with ViT-B/32 . Bold numbers indicate the best F1.

Methods	**Sub-1**	**Sub-2**	**Sub-3**	**Sub-4**	**Sub-5**	**Sub-6**	**Sub-7**	**Sub-8**	**Sub-9**	**Sub-10**	**Average**
Src_only	47.10	35.56	58.12	50.98	51.28	38.76	45.05	38.29	44.14	40.72	45.00
SHOT	44.38	41.85	52.08	47.99	50.53	36.14	43.75	47.35	43.75	39.09	44.69
DSFDA	62.28	59.07	76.36	72.00	76.05	57.16	69.43	66.61	**61.52**	55.95	65.66
SFIT	59.35	58.40	73.29	68.28	68.95	53.84	67.72	63.15	55.29	51.63	62.00
SFDA-IT	61.18	62.58	76.87	70.63	**78.07**	57.65	69.57	56.39	58.06	53.27	64.43
PFT (Ours)	**68.23**	**62.91**	**79.93**	**72.22**	**78.07**	**59.81**	**74.96**	**66.64**	60.26	**56.18**	**67.92**

Table 14: Comparison of the proposed PFT with state-of-the-art SFDA methods on the BAH dataset (10 target subjects, 214 source subjects) with ViT-B/32 . Bold numbers indicate the best F1.

Methods	**Sub-1**	**Sub-2**	**Sub-3**	**Sub-4**	**Sub-5**	**Sub-6**	**Sub-7**	**Sub-8**	**Sub-9**	**Sub-10**	**Average**
Src_only	17.09	12.90	21.09	18.50	18.61	14.07	16.35	13.90	16.02	14.78	16.33
SHOT	42.68	40.25	50.09	46.16	48.60	34.76	42.08	45.55	42.08	37.56	42.98
DSFDA	45.23	42.89	55.44	52.29	55.23	41.49	50.43	48.35	44.63	40.62	47.66
SFIT	47.89	47.10	59.08	55.08	55.60	43.41	54.61	50.96	44.62	41.64	50.00
SFDA-IT	48.22	49.39	60.62	55.73	59.92	45.47	54.87	44.48	45.79	42.01	50.65
PFT (Ours)	**55.75**	**51.41**	**65.31**	**59.01**	**63.79**	**48.87**	**61.26**	**54.45**	**49.24**	**45.91**	**55.50**

Table 15: Comparison of the proposed PFT with state-of-the-art SFDA methods on the BioVid dataset (10 target subjects, 77 source subjects) with ResNet-50. Bold numbers indicate the best F1.

Methods	**Sub-1**	**Sub-2**	**Sub-3**	**Sub-4**	**Sub-5**	**Sub-6**	**Sub-7**	**Sub-8**	**Sub-9**	**Sub-10**	**Average**
Src_only	65.00	53.23	79.56	68.88	72.66	53.00	65.00	55.66	63.22	54.69	63.09
SHOT	70.00	65.89	87.50	78.22	79.11	61.23	73.56	67.77	64.55	56.00	70.38
DSFDA	70.89	68.90	87.00	80.00	79.76	62.55	75.47	70.00	64.76	55.50	71.48
SFIT	75.02	69.00	88.65	80.00	80.14	62.50	81.95	72.45	64.80	60.00	73.45
SFDA-IT	76.25	69.00	88.65	80.69	80.00	62.00	81.50	72.45	65.80	60.40	73.67
PFT (Ours)	**80.00**	**71.50**	**90.20**	**81.50**	**88.10**	**67.50**	**84.60**	**75.20**	**68.00**	**63.40**	**77.00**

Table 16: Comparison of the proposed PFT with state-of-the-art SFDA methods on the StressID dataset (10 target subjects, 44 source subjects) with ResNet-50. Bold numbers indicate the best F1.

Methods	**Sub-1**	**Sub-2**	**Sub-3**	**Sub-4**	**Sub-5**	**Sub-6**	**Sub-7**	**Sub-8**	**Sub-9**	**Sub-10**	**Average**
Src_only	49.22	37.00	56.54	51.11	51.28	40.69	50.89	40.18	42.56	45.44	46.49
SHOT	50.69	42.89	58.00	52.00	51.99	46.14	51.26	45.99	44.05	47.04	49.01
DSFDA	63.00	57.00	75.00	71.97	75.99	52.78	57.77	**69.00**	53.66	46.44	62.26
SFIT	58.69	57.46	73.00	69.78	76.00	57.36	69.69	65.89	57.69	52.00	63.76
SFDA-IT	61.00	60.55	75.75	70.00	77.11	56.65	70.07	66.30	58.66	55.00	65.11
PFT (Ours)	**67.22**	**63.91**	**77.06**	**72.22**	**79.00**	**60.89**	**76.66**	67.60	**59.99**	**58.00**	**68.26**

Table 17: Comparison of the proposed PFT with state-of-the-art SFDA methods on the BAH dataset (10 target subjects, 214 source subjects) with ResNet-50. Bold numbers indicate the best F1.

Methods	**Sub-1**	**Sub-2**	**Sub-3**	**Sub-4**	**Sub-5**	**Sub-6**	**Sub-7**	**Sub-8**	**Sub-9**	**Sub-10**	**Average**
Src_only	16.00	12.07	23.11	18.01	18.96	14.99	17.22	13.44	16.09	15.02	16.49
SHOT	42.98	40.69	51.78	48.00	48.55	40.00	45.87	44.50	43.88	39.99	44.62
DSFDA	45.44	44.00	58.97	54.01	54.00	43.33	51.12	48.99	45.00	40.19	48.51
SFIT	45.76	46.66	59.28	56.01	55.33	44.98	54.00	49.15	44.25	41.14	49.66
SFDA-IT	45.95	47.00	61.11	55.22	55.58	45.45	58.11	49.88	46.08	43.00	50.74
PFT (Ours)	**53.98**	**53.00**	**65.33**	**57.77**	**64.77**	**52.14**	**61.00**	**54.68**	**48.76**	**45.00**	**55.64**

Table 18: Impact of source layer selection for style transfer on classification accuracy (%) using our proposed PFT method for BioVid dataset.

Layer Configuration	**Accuracy (%)**
Layer 1	74.13
Layers 1–2	76.37
Layers 1–3	**82.46**
Last Layers	69.25

Table 19: Average target-domain classification accuracy (%) of SFDA-IT (Hou & Zheng, 2021a) and our proposed PFT methods using different expression loss functions on the BioVid dataset.

expression Loss Type	Image-based	Feature-based
MSE	73.15	77.91
Cross-Entropy	74.20	79.83
KL Divergence	**75.54**	**82.46**

D.5 Source Layer Selection for Style Transfer

To assess the impact of style extraction depth, we experiment with using mean and variance statistics from different layers of the source model to transfer identity-specific information. As shown in Table 18, utilizing only early layers (e.g., Layer 1) yields moderate performance, while progressively including Layers 2 and 3 leads to significant improvements. This suggests that intermediate layers better capture subject-specific style without entangling high-level semantic content. In contrast, using the last layers results in a drop in accuracy, likely due to the abstraction of expression-related features. Overall, these findings highlight the importance of selecting appropriate layers for effective style modeling in source-free FER.

D.6 Effect of expression Loss Type

To evaluate the impact of different expression loss formulations, we compare mean squared error (MSE), cross-entropy (CE), and Kullback–Leibler (KL) divergence in both image-based and feature-based settings. As shown in Table 19, the feature-based model consistently outperforms its image-based counterpart across all loss types, further validating the advantages of operating in the latent feature space. Among the expression loss variants, KL divergence achieves the highest accuracy in both models, suggesting its strength in aligning soft expression distributions more effectively than point-wise (MSE) or hard-target (CE) alternatives. Notably, the feature-based model with KL divergence reaches 80.54% accuracy, outperforming the best image-based counterpart by over 5%, while also benefiting from reduced training cost and model complexity.

E Hyperparameter Details

This section summarizes the hyperparameters used for both source pre-training and target adaptation, as presented in Table 20. We report settings for optimizer types, learning rate schedules, and batch sizes. All experiments use a fixed ResNet-18 backbone to ensure fair comparison across

Table 20: Hyper-parameters for source training and target adaptation.

Hyper-parameter	**Source Training**	**Target Adaptation**
Backbone	`ResNet-18`	`ResNet-18`
Optimizer	SGD + Nesterov	Adam
Momentum	$\{0.1, 0.4, 0.9\}$	NA
Weight Decay	0.0001	0
Learning Rate	$\{0.001, 0.01, 0.02, 0.1\}$	$\{0.0001, 0.001, 0.002\}$
LR Decay Schedule	Step decay at $\{150, 250, 350\}$	ReduceLROnPlateau (patience=3)
Mini-batch Size	$\{32, 64\}$	$\{32, 64\}$
Epochs	$\{30, 50, 100\}$	$\{20, 50\}$
Random Flip	Horizontal/Vertical	Horizontal/Vertical
Color Jitter	Brightness/Contrast/Saturation $= 0.5$, Hue $= 0.05$	Same
Image Size	Resize to 225×225, crop 224×224	Same

methods. The chosen values follow standard SFDA practices and are selected based on source-domain validation performance.